# Intervalence transverse-electric mode terahertz lasing without population inversion

M. F. Pereira, Jr.*
*Materials and Engineering Research Institute, Sheffield Hallam University, Howard Street, Sheffield S1 1WB, United Kingdom*
(Received 25 September 2008; revised manuscript received 3 November 2008; published 5 December 2008)

This paper applies the Keldysh nonequilibrium Green's-function formalism to introduce the concept of *k*-space filtering due to the strong localization of the intervalence transverse-electric (TE) dipole moments in III-V quantum wells. The effect enhances the gain without inversion for holes under nonequilibrium conditions that results from the strong valence-band nonparabolicity and can potentially lead to terahertz lasing at high temperatures. Numerical solutions of the integrodifferential susceptibility equation derived from the microscopic carrier Green's functions are discussed. The approach consistently takes into account the interplay of nonequilibrium nonparabolicity many-body, and dephasing effects as well as the detrimental influence of cross absorption due to the multiple subband transitions.

DOI: 10.1103/PhysRevB.78.245305 PACS number(s): 42.55.Px, 71.20.Nr, 73.21.Fg, 78.66.−w

## I. INTRODUCTION

Intersubband gain without population inversion is a very important topic of current research.[1–4] It is both an extremely elegant phenomenon from the basic physics point of view and crucial for applications due to the difficulty in achieving population inversion at high temperatures in quantum cascade lasers (qcls), which are the main candidates for multipurpose terahertz sources.[5] The fundamental reason underlying this difficulty is that scattering and dephasing processes lead to level broadenings with the same order of magnitude as the lasing transitions, making population inversion by carrier injection in upper lasing subbands extremely difficult in contrast to midinfrared structures as illustrated in Fig. 1.

A mechanism that can indeed lead to room-temperature gain under such restrictive conditions would have a tremendous impact in science and technology due to the wide scope of applications waiting for efficient sources. This is a challenge for advanced quantum mechanics and the first realizations relied on the nonparabolicity of the conduction subbands and local population inversion near $k=0$ even though the lowest subband may have larger global occupation.[3] Different approaches have been recently investigated, e.g., scattering processes broaden the gain transitions allowing for gain without inversion by means of inhomogeneous occupation of the broadened levels.[1] Although inclusion of the nonparabolicity was also important to achieve a good correspondence between the shape of the experimental data and the theory, the key feature needed to predict both the dispersive shape and the right magnitude of the gain curve in the recent experiments of Ref. 2 is actually the Bloch component of the second-order gain and not the nonparabolicity. This is consistent with the approach of Ref. 4.

This paper focuses on the injection of holes in the valence bands of III-V quantum wells. The subband dispersions cannot be described by *k*-independent effective masses due to the strong nonparabolicity of the valence bands. Note that the concept of using nonparabolicity and even a negative mass to produce gain in the valence band of a *p*-type semiconductor has been investigated previously in the literature in Refs. 6 and 7 for the Si/SiGe material system after the concept has been introduced in Ref. 8 for III-V systems. Electroluminescence of quantum cascade structures was reported in Ref. 9 and more recently in Refs. 10 and 11. However lasing has not yet been demonstrated. Si/SiGe qcls are potentially very interesting since they allow easy integration in Si-based electronics. Progress in determining the material parameters for simulations of this system has been recently achieved,[12] but a full picture of all parameters required for predictive calculations of optical properties of Si/SiGe is still not available. This paper is thus based on the GaAs-AlGaAs system where the material parameters are very well known and the growth/processing technology is mature.

Before proceeding further it is useful to summarize unique features of this study of valence-band-based gain without inversion not previously found in the literature.

(i) Although the manipulation of valence-band nonparabolicities and negative masses have been investigated in the literature, the explicit relevance of the TE dipole moment *k* dependence for lasing without inversion has been so far ignored. The constant value of the transition dipole moment used in the calculations is explicitly given in Ref. 7. In contrast, this paper shows that the strongly *k*-dependent TE transition dipole moment can be turned into a unique design tool, i.e., a *k*-space filter that selects the region of *k* space where local inversion takes place. This increases the efficiency of lasing without inversion due to band nonparabolicity and negative masses. Furthermore, previous numerical studies and experimental realizations required low temperatures, while in judicious application this *k*-space filter effect may lead to room-temperature operation.

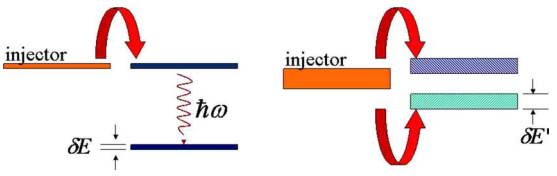


FIG. 1. (Color online) Cartoon of population injection in midinfrared (left) vs terahertz (right) structures. Population inversion can be easily achieved on the left but not on the right. In this case, the electrons can tunnel to either the upper or lower levels: it is difficult to achieve population inversion in terahertz intersubband–based devices.

 

(ii) The nonequilibrium Keldysh Green's-function (NEGF) approach is used to model those systems. The influence of scattering and dephasing mechanisms in the actual gain spectra is thus systematically evaluated, in contrast with the pioneering work in Refs. 6–8 on intervalence gain without inversion due to negative effective masses. The gain in these previous papers has been calculated through direct application of Eq. 5 of Ref. 8 which is the Fermi-golden-rule type in which the Lorentzian function characterizing the spectral broadening is replaced by a Dirac-delta function, assuming that the dephasing is negligible. This unrealistic approach strongly overestimates the gain due to the negative mass region in $k$ space by neglecting contributions from the remaining $k$ space in which the system is not locally inverted.

(iii) Cross absorption to empty subbands can be strongly detrimental and eliminates the gain. This is considered in detail here in contrast with the previous literature in which the intervalence lasing without inversion is overestimated by considering only the gain transition.

Another advantage of the approach presented here is that transverse-electric (TE) polarization is required since the transverse-magnetic (TM) mode does not display the strong localization in $k$ space needed for the filter effect. The TE mode can potentially lead to terahertz surface emission with a simple design in contrast with current developments that are based on TM conduction-band transitions coupled to a complex photonic crystal structure.[13]

The conclusions that stem from the numerical analysis are thus unique to the simulation method used here, in which the complex $k$ dependence of dipole moments and hole dispersion relations can be consistently treated together with a hierarchy of scattering and dephasing mechanisms by expanding the Green's functions in terms of the solutions of an $8\times 8$ $\mathbf{k}\cdot\mathbf{p}$ Hamiltonian. Details of the NEGF method and the interplay of nonparabolicity many-body effects and different scattering mechanisms can be found in Refs. 14 and 15. Reviews of the NEGF formalism in transport in optics of intersubband structures and devices is given, e.g., in Refs. 16–20.

## II. NUMERICAL RESULTS AND DISCUSSION

The absorption $\alpha(\omega)$ and gain spectra $g(\omega)=-\alpha(\omega)$ are calculated from the imaginary part of the optical susceptibility $\chi(\omega)$,

$$\alpha(\omega)=\frac{4\pi\omega}{cn_b}\Im\{\chi(\omega)\},\quad \chi(\omega)=2\sum_{\mu\neq\nu,\vec{k}}\wp_{\mu\nu}(k)\chi_{\nu,\mu}(k,\omega). \tag{1}$$

Here $n_b$ denotes the background refractive index, $c$ is the speed of light, $\wp_{\nu\mu}(k)=ed_{\nu\mu}(k)$ is the transition dipole moment between the subbands $\nu$ and $\mu$, which are labeled $\mu=1,2,\ldots$ from the top valence band. Thus in the discussion that follows, if holes are injected in the second subband and make a transition to subband 1 creating a photon, this actually means that an electron made a transition from valence subband 1 to subband 2 and will be called a (2,1) transition.

The nonequilibrium steady-state susceptibility function $\chi_{\nu\mu}(k,\omega)$ is evaluated through the carriers Keldysh Green's function $G$ whose time evolution is described by a Dyson equation. The resulting integrodifferential equation for $\chi_{\nu\mu}(k,\omega)$ is solved numerically in this paper including many-body effects at the Hartree-Fock level, complex nonparabolic band structure, correlation, and dephasing mechanisms,

$$[\hbar\omega-e_{\nu\mu}(k)+i\Gamma_{\nu\mu}]\chi_{\nu\mu}(k,\omega)-\delta n_{\nu\mu k}\sum_{\mathbf{k}'\neq\mathbf{k}}\chi_{\nu\mu}(k',\omega)\tilde{V}^{\nu\mu}_{\mathbf{k}-\mathbf{k}'}=\wp_{\nu\mu}(k)\delta n_{\nu\mu k}, \tag{2}$$

where $\delta n_{\nu\mu k}=n_\nu(k)-n_\mu(k)$ denotes the nonequilibrium population difference between subbands $\nu$ and $\mu$. Further details of the renormalized energies $e_{\nu\mu}$, electron-electron scattering broadening $\Gamma_{\nu\mu}$, and the Coulomb matrix elements $\tilde{V}^{\nu\mu}_{\mathbf{k}-\mathbf{k}'}$ are given in Refs. 14 and 15.

The model system actually investigated in this paper is globally out of equilibrium but the holes are assumed to be thermalized within each subband with occupation functions characterized by different temperatures, which in turn can be extremely different from the lattice temperature similarly to the case of electrons in conduction-band-based qcls as found in microprobe photoluminescence experiments.[21] Only the two first subbands are occupied and the total number of carriers can be controlled by either optical pumping, selective doping, or a combination of both. There is no global population inversion, with $n_2\leq n_1$ in all cases, where $n_j=\Sigma_{\mathbf{k}}n_j(k)$.

The numerical scheme used here can be summarized as follows. The first step is the solution of the $8\times 8$ $\mathbf{k}\cdot\mathbf{p}$ Hamiltonian.[14,22,23] The Green's functions and self-energies are expanded using eigenstates and eigenvalues of this Hamiltonian. Next, by assuming thermalized holes, the full NEGF scheme is simplified and reduces to the self-consistent evaluation of chemical potentials and self-energy matrix elements which lead to subband energy renormalizations, dephasing constants, and occupation functions. Only carrier-carrier scattering is considered here and details of the corresponding self-energy are given in Ref. 14. Finally, absorption and gain are given by the solution of the integrodifferential equation obtained from the carriers Green's function in linear response and summarized in Eqs. (1) and (2). Solutions of Eq. (2) are obtained by numerical matrix inversion. In other words, the susceptibility function can be written as

$$\chi_{\nu\mu}(k,\omega)=\sum_{\mathbf{k}'\neq\mathbf{k}}(M^{\nu\mu}_{kk'})^{-1}\wp_{\nu\mu}(k')\delta n_{\nu\mu k'}, \tag{3}$$

where $(M^{\nu\mu}_{k'k})^{-1}$ is the inverse of the matrix defined by Eq. (2),

$$M^{\nu\mu}_{kk'}=[\hbar\omega-e_{\nu\mu}(k)+i\Gamma_{\nu\mu}]\delta_{k,k'}+(1-\delta_{k,k'})\delta n_{\nu\mu k}\tilde{V}^{\nu\mu}_{\mathbf{k}-\mathbf{k}'}. \tag{4}$$

The role of the dipole function $\wp_{\nu\mu}(k')$ as a $k$-space filter is then clear in Eq. (3). The overlap of a strongly peaked dipole function exactly where local population inversion $\delta n_{\nu\mu k'}$ takes place enhances the gain without inversion effect as illustrated by Figs. 2 and 3.

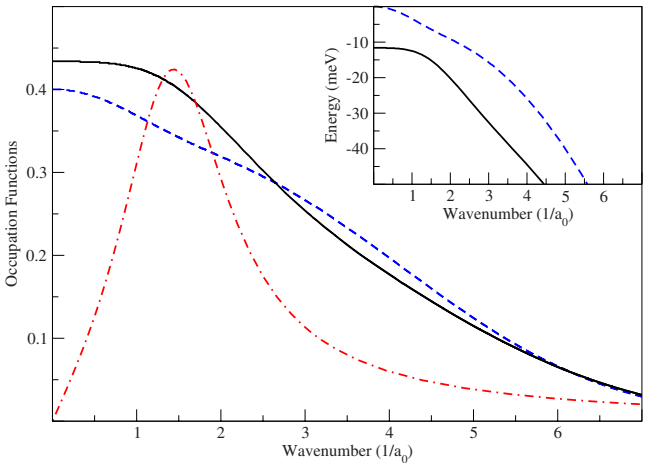


FIG. 2. (Color online) The main part of the plot shows the hole occupation functions (probability of occupation of the subband at a given point in $k$ space) of the top two valence subbands of a 10 nm GaAs-$Al_{0.3}Ga_{0.7}As$ quantum well. The electronic temperature in both subbands is $T=300$ K and both have the same occupation $n_1=n_2=2\times10^{12}$ carriers/cm$^2$. The dashed and solid curves are respectively for $n_1(k)$ and $n_2(k)$ with the corresponding valence bands shown in the inset with the same convention for curves. The dot-dashed line is the transition dipole in nm $[d_{12}(k)=\wp_{12}(k)/e]$ scaled down by a factor of 10 to fit in the figure. The dipole is highly concentrated around $k=1.5$ leading to the $k$-space filter effect discussed in the main body of the paper.

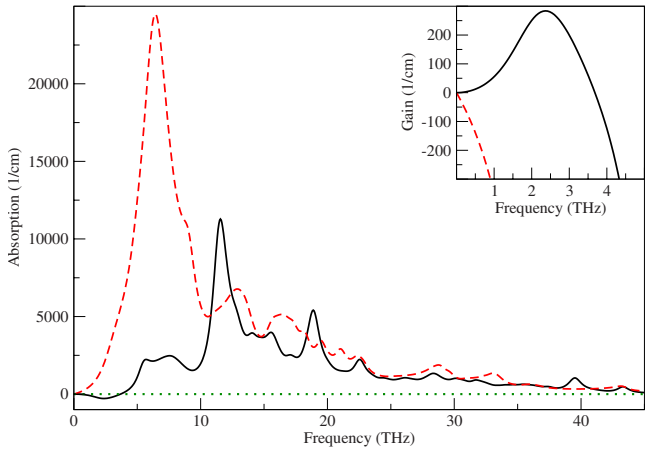


FIG. 3. (Color online) TE absorption spectrum. The electronic temperature in both subbands is $T=300$ K and both have the same occupation $n_1=n_2=2\times10^{12}$ carriers/cm$^2$, which correspond, respectively, to the solid and dashed curves in Fig. 2. Here, the solid absorption curve has been calculated with the full momentum dependence for all transitions; the (2,1) dipole is illustrated by a dot-dashed curve in Fig. 2. In the dashed curve the actual dipoles have been replaced by constants, i.e., the maximum value of each transition dipole. The inset shows in detail the low-frequency region where gain (absorption $\times-1$) develops. In other words, $k$-space filtering is included in the solid curve by means of the actual dipole moment leading to terahertz gain. It is not taken into account in the dashed curve and the gain disappears. The horizontal dotted line is a guide to eyes. It separates the absorption from the gain region between 0 and 3.67 THz.

An actual lasing device will need effective injection of carriers in the upper lasing subband and fast depopulation of the lower laser subband as in a more complex multiple quantum well or superlattice structure operating such as a qcl,[1,2] but the goal of this paper is not that of giving an actual qcl design but rather to focus on the microscopic mechanism to be exploited. Thus, in order to make the analysis of the design tool introduced here as clear and simple as possible, the numerical results presented are for 10 nm GaAs-$Al_{0.3}Ga_{0.7}As$ isolated quantum wells.

However, before proceeding to the full numerical analysis of the isolated well case, a brief qualitative discussion of the implications of the approach introduced here for the design of new terahertz qcls operating at higher temperatures is in order.

The easiest design strategy to bridge the gap between the simple isolated well problem studied here to a full qcl structure is to focus on active regions with single wells and to search for combinations of well and barrier widths and compositions that maximize the local inversion through nonparabolicity and effective filtering of this region. Thicker active regions would maximize the effect but the increased number of transitions can potentially lead to cross absorption losses. Thus, for each target frequency a compromise active region width must be found.

A realistic injector region for efficiently populating the upper laser level will be designed with an upgraded NEGF simulator currently under development. A possible route is to engineer a large miniband acting as a relaxation/injection region, e.g., through strongly coupled heavy hole states as in the Si/SiGe design of Ref. 10 where electroluminescence has been measured. However, in the terahertz range many-body effects can be of the same order of magnitude as the transitions energy and that may affect efficient injection strongly in contrast to midinfrared devices.[15] Furthermore carrier-carrier scattering should play a more important role in the midinfrared case. The current NEGF simulators for qcls do not take into account details of the interplay between many-body and band coupling effects and do not include carrier-carrrier scattering.[15,24,25] Therefore, they cannot be used. Band coupling is required for two reasons. (i) To obtain the $k$-space filtering effect proposed here. (ii) Calculations of the tunneling time of holes in GaAs/AlAs double-barrier heterostructures show clearly that mixing plays a very important role in hole tunneling. In particular conventional effective-mass models can significantly overestimate the heavy-hole tunneling time and thus are not suitable for estimation of the hole tunneling time.[26]

For conduction-band designs the nonparabolicity can be accurately expressed in terms of parabolic dispersions for the subbands, each with different masses. In contrast, the inset in Fig. 2 illustrates the fact that valence subband dispersions can be so strongly $k$ dependent that constant effective masses are not accurate. A general trend of the band coupling effect is the increase in the heavy-hole 1 (subband 1) average effective mass over the value given by the diagonal (parabolic) approximation. The light-hole band (subband 2) can thus have a lower average effective mass, facilitating the laser without inversion effect. The most striking feature of TE-based valence subband transitions is the strong localization

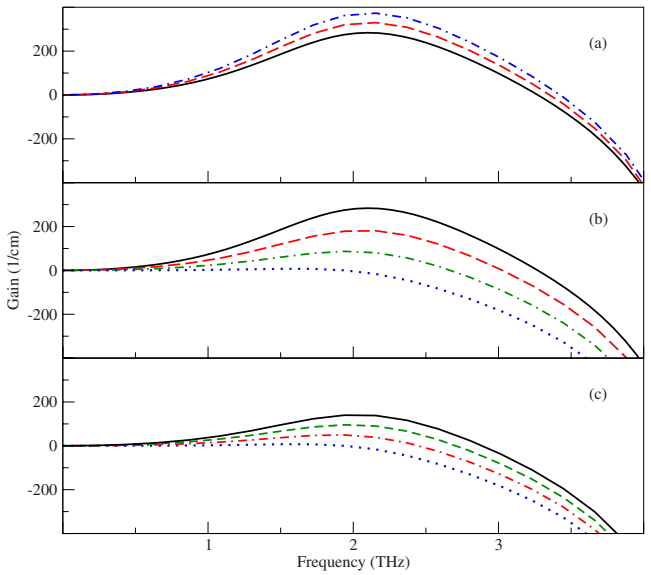


FIG. 4. (Color online) TE gain spectrum. (a) Both subbands have the same carrier density $n_1=n_2=2\times10^{12}$ carriers/cm$^2$. The top hole subband temperature is $T_2=300$ K. The solid, dashed, and dot-dashed curves correspond, respectively, to lower subband temperatures $T_1=300$, 310, and 320 K. (b) Here the holes at both subbands are at the same temperature $T_1=T_2=300$ K. The top subband has a density $n_2=2\times10^{12}$ carriers/cm$^2$, while from top to bottom, the solid, dashed, dot-dashed, and dotted curves correspond, respectively, to lower subband densities $n_1=2$, 2.1, 2.2, and 2.3 $\times10^{12}$ carriers/cm$^2$. (c) All curves have the first and second subband occupations given, respectively, by $n_1=2.3\times10^{12}$ carriers/cm$^2$ and $n_2=2\times10^{12}$ carriers/cm$^2$ and $T_2=300$ K. The dotted line represents the same curve as in (b), i.e., $T_1=300$. The lower subband temperature is progressively raised from bottom to top. The dot-dashed, dashed, and solid curves correspond, respectively, to $T_1=310$, 320, and 330 K.

of the transition dipoles in $k$ space shown by the dot-dashed curve in Fig. 2.

This amazing feature allows the use of the dipoles as filters for the regions in $k$ space where the system is locally inverted. Indeed, Fig. 3 shows that if we replace the strongly $k$-dependent dipole moments by constant effective values, as in the dashed curves, where $\wp_{\nu\mu,\mathrm{eff}}=\max\{\wp_{\nu\mu}(k)\}$, all of $k$ space contributes and the gain without inversion disappears in contrast to the full $k$-dependent calculation (solid curve) that clearly shows gain (negative absorption) in the low-energy side of the spectrum. All calculations presented here take into account possible cross absorption to higher subbands as the multiple absorption peaks show.

An important point should be highlighted at this point. The absorption and gain spectra are inversely proportional to the period length. The period used here is the quantum well width $L_c=10$ nm consistently with the model. In actual qcls, the period is extended to include barriers, injector, and collectors, and it can easily be at least 5× as large. Since the number of photons emitted per period remains constant this means that the gain spectra calculated here are very high in comparison to what should be expected in actual qcl structures. Note however that the qualitative analysis that follows is fully consistent with the single quantum well model.

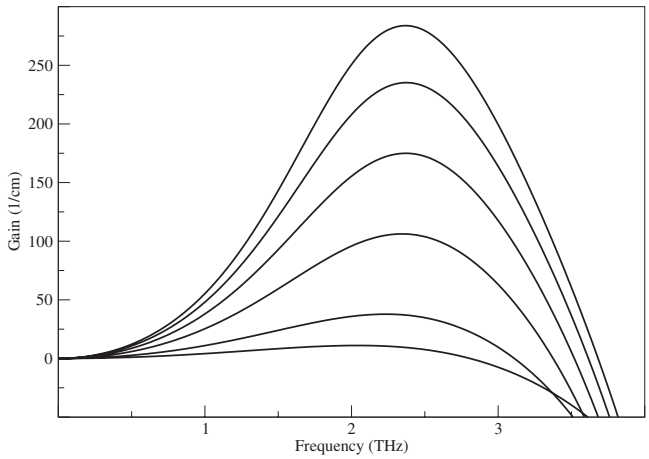


FIG. 5. TE gain spectrum. (a) The carriers in both subband have the same temperature, $T_1=T_2=300$ K, and the same total carrier density. From top to bottom the total carrier density carriers per subband is decreased by $n_1=n_2=2$, 1.6, 1.2, 0.8, 0.4, and 0.2 $\times10^{12}$ carriers/cm$^2$.

Figure 4 shows the low-energy gain region in more detail and illustrates the main features of the gain mechanisms as a function of subband occupation and electronic temperatures. Figure 4(a) confirms the expected results that if the densities on both bands are held the same and the lower subband temperature increases, the gain increases. Figure 4(b) shows that for the same temperature on both subbands, gain without inversion for the structure persists to a certain extent even if the total density of carriers in the lower band increases, which is a very interesting feature. Finally, Fig. 4(c) starts from equal temperatures and the worst case depicted in Fig. 4(b) where the gain disappears. By holding the densities fixed and increasing the lower band temperature, the gain recovers. Cooling mechanisms for one subband with respect

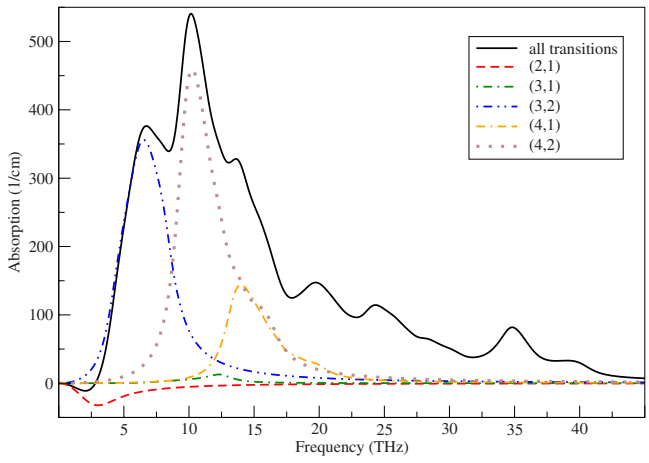


FIG. 6. (Color online) TE absorption spectrum. (a) The carriers in both subband have the same temperature, $T_1=T_2=300$ K, and the same total carrier density $n_1=n_2=2\times10^{11}$ carriers/cm$^2$. The solid curve includes all transitions and from left to right, the dashed, dash-double-dotted, dotted, dot–dashed and dot-double-dashed curves correspond, respectively, to transitions between the final $j$ and initial $i$ subbands $(j,i)=(2,1)$, (3,2), (4,2), (3,1), and (4,1).

to the other will be the subject of future research. The fact that the active region in qcls is typically at a higher temperature than the contacts as shown in Ref. 21 allows a range of temperatures to be manipulated.

In Figs. 3 and 4 the carrier density is quite high to emphasize the filtering effect in isolated quantum wells. In a cascaded structure with a realistic injector, the densities that can be achieved in practice should be smaller. Thus Fig. 5 simulates this by considering the evolution of gain spectra for decreasing equal population density in the occupied subbands. A reduction by 1 order of magnitude in the densities leads to a corresponding reduction in 1 order of magnitude in the peak gain value. The important message is that although reduced, the gain persists and the filtering effect remains effective for smaller and more realistic densities.

Figure 6 shows how cross absorption to empty upper subbands can compete with, and in many cases eliminate, the intersubband gain. The most important transitions that influence the gain region are shown. It is clear that cross absorption strongly reduces the gain due to the (2,1) transition (dashed curve).

In summary, the lasing without inversion concept introduced in this paper by manipulating the occupation functions through band-structure engineering and using the unique $k$ dependence of some intervalence band transitions as a $k$-space filter can potentially lead to revolutionary intersubband lasing designs operating at room temperature in simple surface emitting configurations with TE polarization.

*m.pereira@shu.ac.uk

[1] A. Wacker, Nat. Phys. **3**, 298 (2007).
[2] R. Terazzi, T. Gresch, M. Giovanni, N. Hoyler, F. Faist, and N. Sekine, Nat. Phys. **3**, 329 (2007).
[3] J. Faist, F. Capasso, C. Sirtori, D. L. Sivco, A. L. Hutchinson, M. S. Hybertsen, and A. Y. Cho, Phys. Rev. Lett. **76**, 411 (1996).
[4] H. Willenberg, G. H. Dohler, and J. Faist, Phys. Rev. B **67**, 085315 (2003).
[5] R. Köhler, A. Tredicucci, F. Beltram, H. E. Beere, E. H. Linfield, A. G. Davies, D. A. Ritchie, R. C. Iotti, and F. Rossi, Nature (London) **417**, 156 (2002).
[6] L. Friedman, G. Sun, and A. Soref, Appl. Phys. Lett. **78**, 401 (2001).
[7] R. A. Soref and G. Sun, Appl. Phys. Lett. **79**, 3639 (2001).
[8] G. Sun, A. Liu, and J. B. Khurgin, Appl. Phys. Lett. **72**, 1481 (1998).
[9] G. Dehlinger, L. Diehl, U. Gennser, H. Sigg, J. Faist, K. Ensslin, D. Grutzmacher, and E. Muller, Science **290**, 2277 (2000).
[10] L. Diehl, S. Mentese, E. Müller, D. Grützmacher, H. Sigg, U. Gennser, I. Sagnes, Y. Campidelli, O. Kermarrec, D. Bensahel, and J. Faist, Appl. Phys. Lett. **81**, 4700 (2002).
[11] R. Bates, S. A. Lynch, D. Paul, Z. Ikonic, R. W. Kelsall, P. Harrison, S. L. Liew, D. J. Norris, A. G. Cullis, W. R. Tribe, and D. D. Arnone, Appl. Phys. Lett. **83**, 4092 (2003).
[12] D. J. Paul, Phys. Rev. B **77**, 155323 (2008).
[13] L. Sirigu, R. Terazzi, M. I. Amanti, M. Giovanni, J. Faist, L. Andrea Dubar, and R. Houdre, Opt. Express **16**, 5206 (2008).
[14] M. F. Pereira, Jr. and H. Wenzel, Phys. Rev. B **70**, 205331 (2004).
[15] M. F. Pereira, Jr., S.-C. Lee, and A. Wacker, Phys. Rev. B **69**, 205310 (2004).
[16] A. Wacker, Phys. Rep. **357**, 1 (2002).
[17] S. C. Lee and A. Wacker, Phys. Rev. B **66**, 245314 (2002).
[18] A. Wacker, S.-C. Lee, and M. F. Pereira, Jr., in *Simulation of Transport and Gain in Quantum Cascade Lasers*, edited by B. Kramer, Advances in Solid State Physics Vol. 43 (Springer, Berlin, 2003), p. 369.
[19] H. Haug and A. P. Jauho, *Quantum Transport and Optics of Semiconductors* (Springer, Berlin, 1996).
[20] S. Datta, Superlattices Microstruct. **28**, 253 (2000).
[21] M. S. Vitiello, G. Scamarcio, V. Spagnolo, T. Losco, R. P. Green, A. Tredicucci, H. E. Beere, and D. A. Ritchie, Appl. Phys. Lett. **88**, 241109 (2006).
[22] F. Szmulowicz, Phys. Rev. B **51**, 1613 (1995).
[23] H. Wenzel, G. Erbert, and P. M. Enders, IEEE J. Sel. Top. Quantum Electron. **5**, 637 (1999).
[24] R. Nelander, A. Wacker, M. F. Pereira, Jr., D. G. Revin, M. R. Soulby, L. R. Wilson, J. W. Cockburn, A. B. Krysa, J. S. Roberts, and R. J. Airey, J. Appl. Phys. **102**, 113104 (2007).
[25] T. Kubis, C. Yeh, and P. Vogl, Phys. Status Solidi C **5**, 232 (2008).
[26] M. U. Erdoğan, K. W. Kim, and M. A. Stroscio, Appl. Phys. Lett. **62**, 1423 (1993).